EARTHQUAKE ENGINEERING AND STRUCTURAL DYNAMICS, VOL. 26, 781–795 (1997)

NONLINEAR BEHAVIOUR OF SCORIA SOIL SEDIMENTS EVALUATED FROM BOREHOLE RECORDS IN EASTERN SHIZUOKA PREFECTURE, JAPAN

TOSHIMI SATOH,[1]* MASANORI HORIKE,[2] YOSHIHIRO TAKEUCHI,[2] TOMIICHI UETAKE[3] AND HIDEYO SUZUKI[3]

[1]*Izumi Research Institute, Shimizu Corporation, Fukoku-seimei Bldg. 2-2-2 Uchisaiwai-cho, Chiyoda-ku, Tokyo, 100 Japan*
[2]*Department of Architecture, Osaka Institute of Technology, 5-1-16 Omiya, Asahi-ku, Osaka, 535 Japan*
[3]*Tokyo Electric Power Company, 4-1 Egasaki-cho, Tsurumi-ku, Yokohama, 230 Japan*

SUMMARY

We evaluate the non-linear behaviour of soil sediments, analysing five weak and four strong motions observed at depths of 1 m and 28 m, in eastern Shizuoka prefecture, Japan. We identify S-wave velocities and frequency-dependent damping factors by minimizing the residual between observed and theoretical spectral ratios, based on a linear one-dimensional model. We find that S-wave velocities identified from strong motions, whose peak ground acceleration are 440, 210, 176, and 140 cm/s^2, are significantly smaller than those identified from weak motions. The shear modulus reduction ratios estimated from identified S-wave velocities become clear above an effective shear strain of 10^{-4} and agree with laboratory test results below an effective shear strain of 8×10^{-4}. The differences of damping factors between weak and strong motions are not clear below this effective shear strain, as the laboratory test suggested. The equivalent linear one-dimensional model, with frequency-dependent damping factors, is confirmed to be valid to simulate strong motions at least an effective shear strain of less than 4×10^{-4}. © 1997 by John Wiley & Sons, Ltd.

Earthquake Engng. Struct. Dyn., **26**, 781–795 (1997)

No. of Figures: 10. No. of Tables: 3. No. of References: 27.

KEY WORDS: non-linear; site response; borehole records; system identification; strong ground motion

1. INTRODUCTION

Non-linear site response in sedimentary layers during strong ground shaking has been a controversial issue for a long time. Since the pioneering work done by Seed and Idriss,[1] most geotechnical engineers have recognized non-linear soil response. A number of experimental studies have been carried out to establish the stress–strain behaviour of various types of soil.[2–4] However, in studies based on observed strong motions, some researchers[5,6] show no evidence of non-linearity of soil, while others[7–15] show evidence of it. Darragh and Shakal[16] and Wen *et al.*[17] point out that difference of site responses between weak and strong motions is clear at one soft-soil site, but not at the other stiff-soil site. Midorikawa[18] reviewed many studies on non-linearity of soil and concluded that the effective shear strain level of strong motions used in studies in which no evidence of non-linearity is detected is less than about 3×10^{-4}. This interpretation may answer the question of why evidence of non-linearity of soil is sometimes clear, sometimes not. He also pointed out, by comparing a result from Singh *et al.*[10] with others that Mexico city clay keeps linearity up to a larger effective shear strain level than the other types of soil. Thus, since non-linearity of soil would depend on soil type, such as clay or sand, the non-linearity of soil during strong motions with various effective shear strain levels should be confirmed at various sites.

In order to study the non-linearity of soil quantitatively, it is necessary to separate site responses from observed records, because observed records include effects of source and path, as well as site responses. Chin

* Correspondence to: Toshimi Satoh, Izumi Research Institute, Shimizu Corporation, Fukoku-seimei Bldg. 2-2-2 Uchisaiwai-cho, Chiyoda-ku, Tokyo, 100 Japan

CCC 0098–8847/97/080781–15$17·50

Received 31 October 1995
Revised 7 November 1996

and Aki,[7] Kamiyama,[8] and Yamamoto *et al.*[9] show the evidence of non-linearity of soil by separating site responses from strong motions records observed on the surface. Many researchers[6,10–12,16] assume spectral ratios between rock and soil sites to be site responses, and claim that the difference of spectral ratios of weak motions from those of strong motions show the existence of non-linearity of soil sediments. This assumption, however, is not always good because the input motion to a soil site is different from that to a distant rock site, and furthermore seismic motions at a rock site are disturbed by the effect of near-surface weathering and topography.

Borehole records, however, give us more direct and reliable site responses than the methods outlined above because site responses can be evaluated directly by calculating spectral ratios between surface and borehole motions[13–15,17]. Chang *et al.*[13] and Wen[14] evaluated the non-linear behaviour of soil sediments from S-wave velocities estimated under the assumption of a simple two-layered soil model, using surface and borehole records in Taiwan. Chang *et al.*[13] pointed out that the relation between the shear modulus reduction ratio and the shear strain estimated from the spectral ratios agrees with laboratory test results in the effective shear strain range between 3×10^{-4} and 2×10^{-3}. Wen[14] pointed out that the estimated S-wave velocity decreases as Peak Ground Acceleration (PGA) increases. Satoh *et al.*[15] identify not only S-wave velocities but also damping factors by minimizing the residual between observed and theoretical spectral ratios, based on a linear one-dimensional (1-D) model using surface and borehole records in Japan. Although they evaluated non-linearity of soil quantitatively, their data were only one strong motion and three weak motions.

An observation site of weak and strong motions was set up in eastern Shizuoka prefecture, Japan, in 1977. The records observed there are suitable for researching the non-linear behaviour of soil sediments quantitatively because of the following conditions: (1) This site has a borehole where accelerometers are installed at depths of 1 and 28 m. (2) Four strong motions and five weak motions were observed. The largest and the second largest PGA among the strong motions were 440 and 210 cm/s^2, respectively. (3) The underground structure up to 160 m was surveyed by P-wave, S-wave and density logging. (4) Dynamic deformation characteristics, that is, the relation between the shear modulus reduction ratio and the shear strain and the relation between the damping factors and the shear strain, were obtained by laboratory tests.

A primary objective of our study is to evaluate the non-linear behaviour of soil sediments as quantitatively as possible. We evaluate the following aspects of the nonlinearity of soil: (1) We calculate spectral ratios between surface and borehole records, and compare the spectral ratios of strong motions with those of weak motions. If the soil behaves non-linearly, we will find peak shifts to a longer period and deamplification of the peak levels in spectral ratios of strong motions compared with weak motions. (2) We estimate S-wave velocities and frequency-dependent damping factors of soil during weak and strong motions and examine if a decrease of S-wave velocities and the increase of damping factors can be seen during strong motions. (3) We estimate effective shear strain based on a linear 1-D model using estimated S-wave velocities and damping factors. Then we compare the dynamic deformation characteristics obtained from estimated S-wave velocities, damping factors, and effective shear strain with those from laboratory tests.

A secondary objective is to examine if the equivalent linear 1-D model using the dynamic deformation characteristics obtained from laboratory tests is useful for strong motion prediction. Therefore, we compare observed strong motions with simulated ones calculated from the equivalent linear 1-D model, using soil constants identified from weak motions and dynamic deformation characteristics obtained from laboratory tests.

2. RECORDING STATIONS AND DATA

Figure 1 shows the location of the observation site in eastern Shizuoka prefecture and epicentres of the nine earthquakes analysed in this study. In 1977, two accelerometers denoted as GL0 and GL28, were installed at depths of 1 and 28 m, respectively. One more accelerometer was installed at a depth of 160 m in 1986. These digital accelerometers, with three components, have flat amplitude response from 0·03 to 30 Hz.

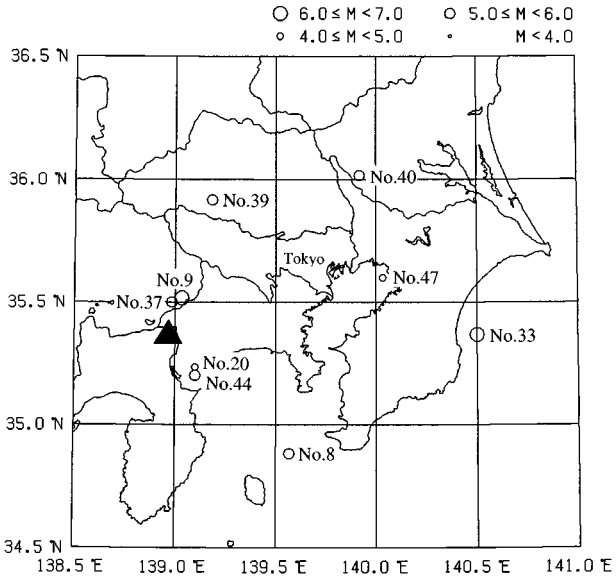

Figure 1. Location of a borehole observation site (a triangle) in eastern Shizuoka prefecture and epicentres of nine earthquakes analysed in this study

Table I. List of earthquakes with parameters determined by the Japan Meteorological Agency and peak ground acceleration at GL0

	Event	Origin time	M_J	Focal depth (km)	Epicentral distance (km)	Peak ground acceleration at GL0 (cm/s^2)		
						NS	EW	UD
No. 8	South off Kanto	1982-8-12 33:33	5·7	30	70	40·5	39·6	19·1
No. 9	Eastern Yamanashi prefecture	1983-8-8 12:47	6·0	22	12	439·6*	—	262·0
No. 20	Hakone region	1986-7-9 01:17	4·1	15	19	28·3	31·1	29·7
No. 33	Kujukuri coast	1987-12-17 11:08	6·7	58	137	75·1	116·9	27·9
No. 37	Eastern Yamanashi prefecture	1988-9-5 00:49	5·6	30	14	212·3	140·0	90·4
No. 39	Western Saitama prefecture	1988-9-29 17:23	5·0	15	62	19·1	16·3	7·0
No. 40	South-west Ibaraki prefecture	1989-2-19 21:27	5·6	55	110	15·2	11·8	6·3
No. 44	Hakone region	1990-8-5 16:13	5·1	14	21	81·3	176·2	44·4
No. 47	Central Chiba prefecture	1991-11-19 17:24	4·9	81	99	21·1	34·5	5·5

*Corrected wave

Table I shows the data of the earthquakes analysed in this study. We consider horizontal records of five earthquakes, whose PGA are between 10 and 40 cm/s^2 to be weak motions, and records of four earthquakes with PGA of their two horizontal components greater than 100 cm/s^2, to be strong motions. We will refer to the earthquakes by the names shown in the first column of Table I. The subsurface soil in eastern Shizuoka prefecture is mainly composed of scoria which is vesicular volcanic soil as shown in Table II. The first,

Table II. Soil profile based on S-wave logging and density logging

Layer	Depth (m)	Soil classification	Density (t/m^3)	S-wave velocity (m/s)
1st layer	~ 5·0	Scoria with Loam	1·46	125
2nd layer	~ 7·0	Kuroboku silt	1·48	130
3rd layer	~ 12·2	Scoria with Loan	1·68	252
4th layer	~ 24·0	Loan with Scoria	1·69	425
5th layer	~ 28·0	Scoria	1·95	780

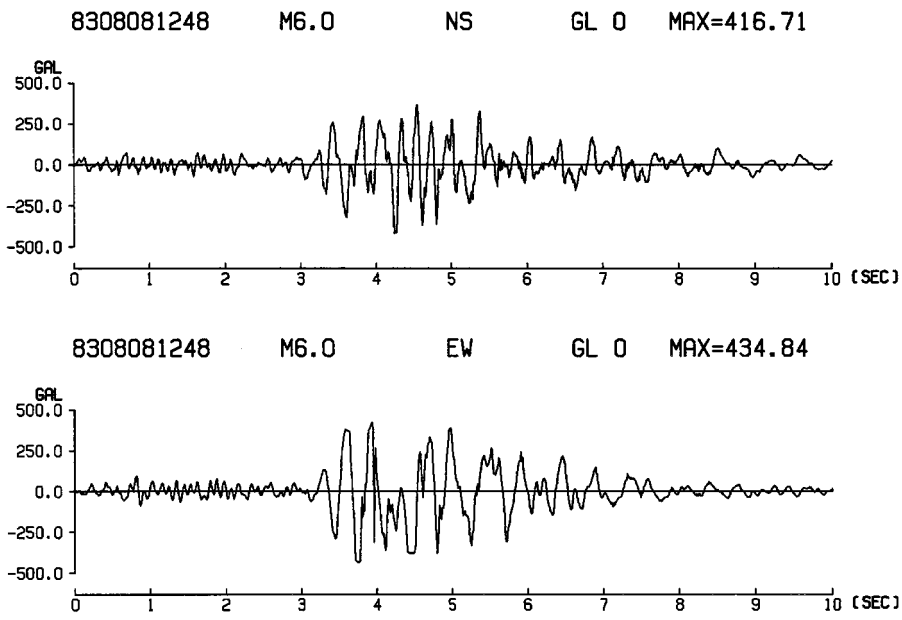

Figure 2. Original accelerograms of NS and EW components for No. 9 observed at GL0

second, and third layers are composed of soft soil sediments, so we can assume that the non-linear behaviour of soil sediments would appear mainly in these three alluvial layers during strong motions. Therefore we analyse horizontal records of GL28 and GL0 and focus our attention on the non-linear behaviour of soil sediments in these three alluvial layers.

The original accelerograms at GL0 for No. 9 are shown in Figure 2. Both horizontal-component accelerograms are saturated. Egawa *et al.*[19] corrected them by interpolating the saturated portions using a polynomial expression. Figure 3 shows the corrected accelerograms at GL0 and original ones at GL28 for No. 9 used in this study. We correct orientation errors of borehole accelerometers estimated by the coherence method.[20]

3. IDENTIFICATION METHOD OF SOIL CONSTANTS

We evaluate the non-linear behaviour of soil sediments from spectral ratios between GL0 and GL28 based on a linear 1-D model in which the underground geological structure is laterally homogeneous and S-waves

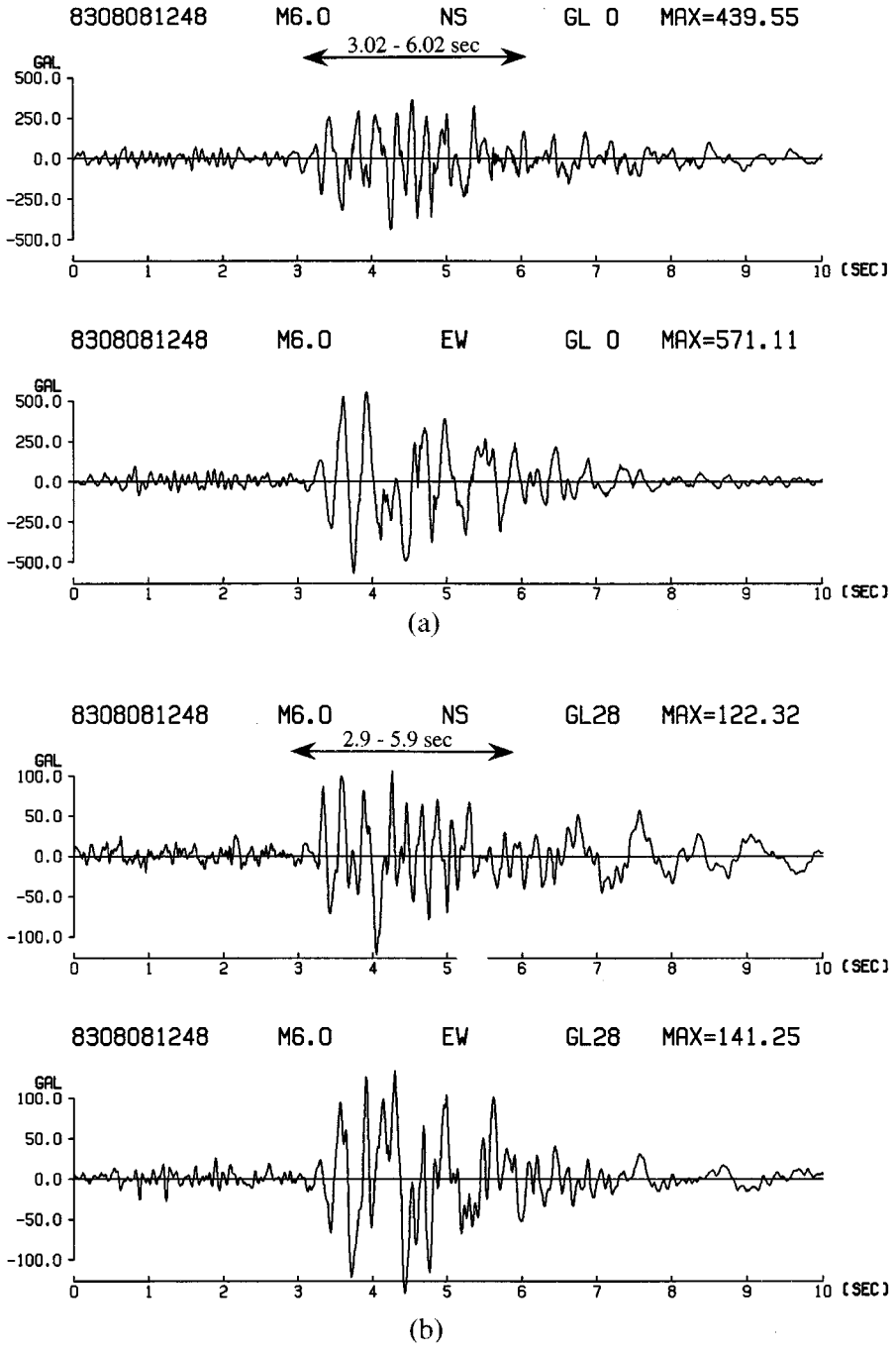

Figure 3. Accelerograms of NS and EW components for No. 9. (a) Accelerograms corrected by Egawa *et al.*[19] observed at GL0 and (b) original accelerograms observed at GL28

are incident vertically. Therefore, in order to calculate spectral ratios for the time segments of S-waves having as high coherence as possible, first we estimate relative time differences between GL0 and GL28 by cross-correlation analysis[21] and then calculate spectral ratios for time segments considering the relative time differences.

We calculate the spectral ratios between GL0 and GL28 and estimate S-wave velocities and frequency-dependent damping factors $h = h_0 f^{-\alpha}$ (f: frequency) by using system identification techniques[15,22–24] to minimize the following criterion function:

$$J(\{r\}) = \frac{\int_{fs}^{fe} |H_0(f) - H_t(f, \{r\})|^2 \, df}{\int_{fs}^{fe} |H_0(f)|^2 \, df} \tag{1}$$

The notation $\{r\}$ is a vector of unknown parameters, $H_0(f)$ is the observed spectral ratio, $H_t(f, \{r\})$ is the theoretical spectral ratio based on the linear 1-D model, and fs and fe are the minimum and maximum frequencies. The theoretical spectral ratio is calculated by SHAKE program[25] in which we assume frequency-dependent damping factors, because Satoh *et al.*[24] showed from a lot of weak motions recorded at twelve different borehole stations that observed spectral ratios can be explained better based on the linear 1-D model by using frequency-dependent damping factors than frequency-independent ones. Here we assume soil below GL28 is half-space. We employ the modified quasi-Newton method[26] to solve the above equation. In this analysis, observed Fourier spectra are smoothed using a Parzen window with 0·4 Hz bandwidth. In the identification procedure we apply the same Parzen window to the theoretical Fourier spectra. We regard S-wave velocities of the first and second layers to be the same, because the difference between them is not large enough to be detected by the identification method. We identify one h_0 and one α in all the layers between GL0 and GL28. There are four unknown parameters in total, namely: the S-wave velocity common to the first and second layers, the S-wave velocity of the third layer, h_0 and α. The logging results shown in Table II are initial values for S-wave velocities for weak motions. We assume initial values of frequency-dependent damping factors to be $0{\cdot}1 f^{-0{\cdot}7}$ for weak motions, based on preliminary analysis. For strong-motion averages of S-wave velocities and damping factors identified from weak motions are used as their initial values. Densities and thicknesses are fixed by values in Table II.

4. RESULTS AND DISCUSSION

4.1. Observed spectral ratios and identified soil constants

We extract S-wave dominant segments from velocity seismograms integrated from accelerograms by using a 3 s window with 0·5 s cosine-shaped tapers at both ends. At this stage the segments of GL0 records are synchronized with GL28 records. The extracted segments are filtered in the frequency range from 1 to 20 Hz just for cross-correlation analysis. Cross-correlation coefficients of these segments between GL28 and GL0 are shown in Figure 4. Note the cross-correration coefficients are calculated by taking GL0 as a reference. It is confirmed that most records have peaks at a time difference of about $-0{\cdot}12$ s except for the EW component of No. 9. This time difference of $-0{\cdot}12$ s agrees with the travel time of S-waves calculated from the S-wave velocity structure in Table II. The reason for the time difference of the EW component of No. 9 being different from the others may be an inappropriate correction of saturated waves, because an abnormal waveform is seen at the time of 4 s in the original wave, as shown in Figure 2. We eliminate the EW component of No. 9 from the following analysis for these reasons. For the other records we extract S-wave segments of accelerograms by considering the time difference of $-0{\cdot}12$ s as shown by arrows in Figure 3. Then the spectral ratio between GL0 and GL28 is calculated for each pair of the S-wave segments. We use the NS component of No. 9 corrected by Egawa *et al.*,[19] because we confirm that the difference between the original and corrected spectral ratios in the frequency range 1–20 Hz is almost nothing for NS component of No. 9.

Figure 5 shows the spectral ratios of the five weak motions and Figure 6 shows the average of them. The averages of spectral ratios are different between the NS and EW components. Identified S-wave velocities

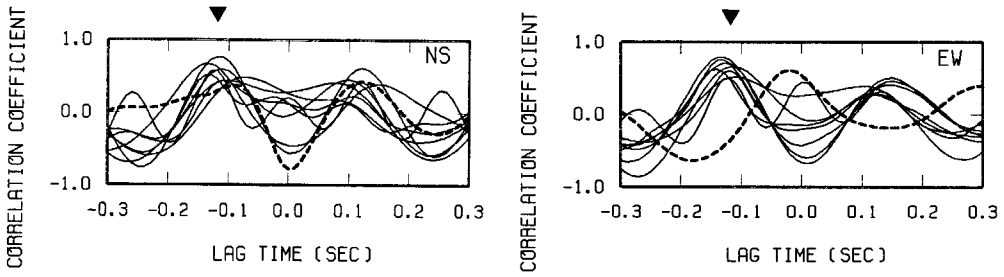

Figure 4. Cross-correlation coefficients between the velocity seismograms at GL0 and GL28 for No. 9 (dashed lines) and the others (thin lines)

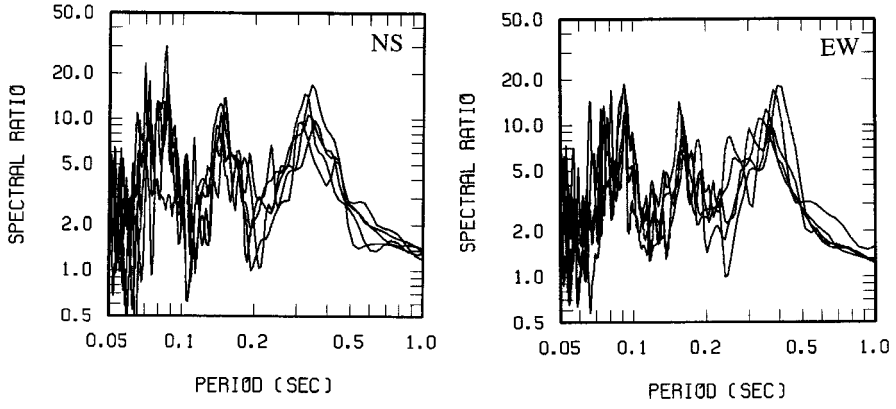

Figure 5. Observed spectral ratios between GL0 and GL28 for weak motions

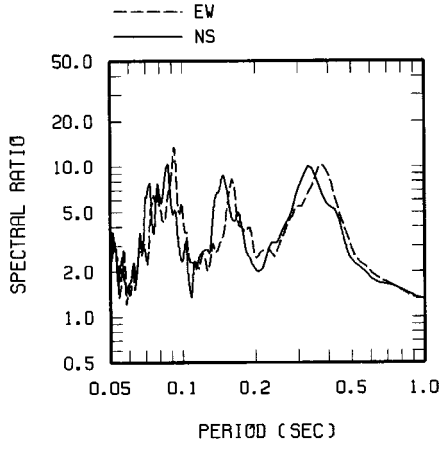

Figure 6. Averages of observed spectral ratios between GL0 and GL28 for weak motions

and damping factors are shown in Table III. It is found that the S-wave velocities for NS components are slightly larger than those for EW components. In this study we use the NS and EW components independently, and not their vector sum of or of their major and minor axes. We do this for two reasons. One is that azimuths of records should not vary with earthquakes, because the difference between them may be due to

Table III. Identified S-wave velocities and frequency-dependent damping factors

	NS				EW			
	S-wave velocity of 1st and 2nd layers	S-wave velocity of 3rd layer	Damping factor $h = h_0 f^{-\alpha}$		S-wave velocity of 1st and 2nd layers	S-wave velocity of 3rd layer	Damping factor $h = h_0 f^{-\alpha}$	
Earthquake	(m/s)	(m/s)	h_0	α	(m/s)	(m/s)	h_0	α
No. 8*	132·2	210·0	0·146	0·666	108·4	204·2	0·165	0·743
No. 9	97·8	162·6	0·250	0·868	—	—	—	—
No. 20*	130·0	210·7	0·141	0·741	120·9	202·6	0·226	0·882
No. 33	128·7	209·4	0·278	1·008	117·4	198·2	0·388	1·099
No. 37	115·1	182·5	0·119	0·603	101·6	183·9	0·235	0·768
No. 39*	128·5	209·8	0·165	0·826	114·5	200·3	0·155	0·791
No. 40*	135·9	225·7	0·109	0·760	114·4	204·6	0·309	1·168
No. 44	124·5	219·0	0·429	1·157	107·7	187·8	0·201	0·836
No. 47*	124·0	203·5	0·183	0·586	110·4	201·1	0·200	0·696
Average and standard deviation of weak motions	130·1 ± 4·0	211·9 ± 7·3	0·149 ± 0·025	0·716 ± 0·083	112·9 ± 3·1	202·5 ± 1·7	0·211 ± 0·055	0·856 ± 0·168

* Weak motions

two- or three-dimensional inhomogenity. The other is that the orbits on the horizontal plane do not show predominant polarization.

In Figure 7, observed spectral ratios of the NS components of No. 9 and No. 37 are shown together with the theoretical spectral ratios which are computed based on a linear 1-D model using identified soil constants. It is confirmed that the theoretical spectral ratios are in good agreement with the observed ones. Comparing the averages of the observed spectral ratios of weak motions, it is found that the peak shifts of No. 9 with a PGA of 440 cm/s^2 are larger than those of No. 37 with a PGA of 210 cm/s^2. Identified S-wave velocities of the NS components of No. 9 and No. 37 are significantly smaller than the averages of S-wave velocities identified from weak motions of the NS components. It is also found that the identified S-wave velocities of the EW components of No. 37 with a PGA of 140 cm/s^2 and No. 44 with a PGA of 176 cm/s^2 are significantly smaller than the averages of S-wave velocities identified from the EW components of weak motions.

In Figure 8, criterion function values in equation (1) for the NS component of No. 9 are shown as contour maps. In Figure 8 (a) S-wave velocity of the first and second layers and that of the third layer are changed under the condition that the parameters h_0 and α of the damping factor are fixed values identified from No. 9. In Figure 8(b) h_0 and α of damping factors are changed under the condition that S-wave velocities are fixed values identified from No. 9. Triangles show the S-wave velocities and damping factors identified from No. 9. Circles show the average ones identified from five weak motions. The contour interval in (a) is the same as that in (b). It shows that the variations of the criterion function value between No. 9 and five weak motions in (a) (for changing S-wave velocities) are larger than those in (b) (for changing damping factors). Thus, the sensitivity of damping factors is smaller than that of S-wave velocities.

4.2. Dynamic deformation characteristics

In order to evaluate non-linear behaviour from the dynamic deformation characteristics of soil, we estimate the effective shear strain, which is 65 per cent of the maximum shear strain,[25] based on a linear 1-D model using S-wave velocities and frequency-dependent damping factors identified from the records of interest.

By considering laboratory test results and the effective shear strain estimated from the five weak motions, we assume that the shear modulus reduction ratio calculated from the average of S-wave velocities identified

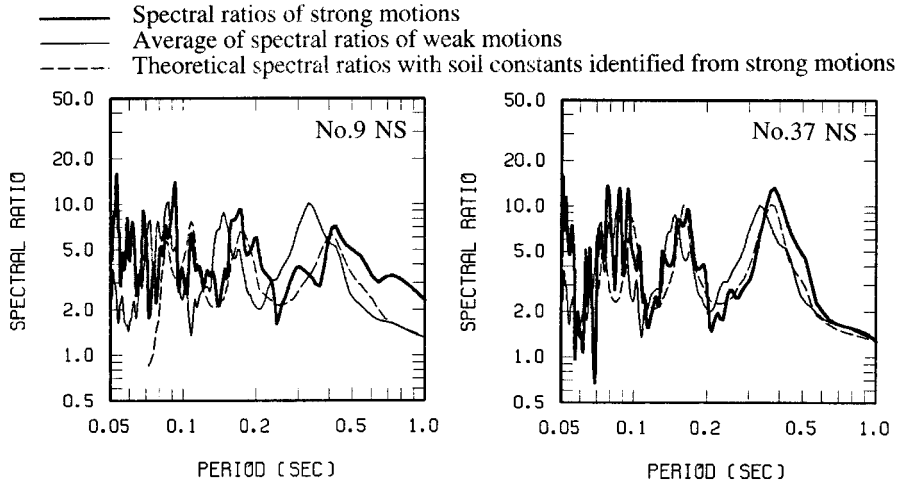

Figure 7. Observed (thick lines) and identified (dashed lines) spectral ratios between GL0 and GL28 of strong motions and the average of spectral ratios of weak motions (thin lines)

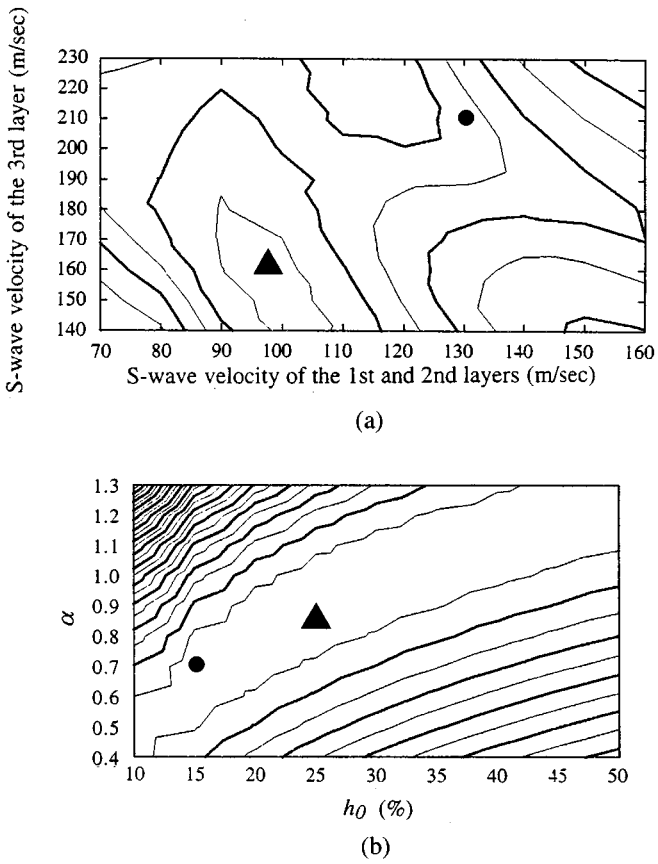

Figure 8. Values of criterion function in equation (1) for the NS components of No. 9. Triangles show the S-wave velocities and damping factors identified from No. 9. Circles show the average ones identified from five weak motions

from the weak motions is 0·93. Shear modulus reduction ratios are calculated from the power of the ratios between S-wave velocities identified from observed spectral ratios and those at the effective shear strain of 10^{-6}. In Figure 9 we show the estimated effective shear strain and shear modulus reduction ratios together with laboratory test results. The estimated shear modulus reduction ratios become clear above an effective shear strain of 10^{-4} and agree with laboratory test results below an effective shear strain of 8×10^{-4}.

In Figure 9 we show the estimated effective shear strain and damping factors together with laboratory test results. Here we show the damping factors at 3·1 Hz which is the first peak of spectral ratios of weak motions. If non-linear behaviour exists, the increase of damping factors should appear as increasing effective shear strain. Although we cannot see such clear evidences in estimated values below an effective shear strain of 8×10^{-4}, the increase of damping factors obtained from laboratory test is also small in an effective shear strain range of 1×10^{-4} to 8×10^{-4}.

The estimated damping factors and S-wave velocities should vary for different earthquakes even if their effective strains are the same because spectral ratios vary with parameters such as angles of incidence and azimuth, multiply the reflected/refracted body and surface wave contamination, and so on. That is why the identified damping factors and S-wave velocities do not vary smoothly as the increasing effective shear strain.

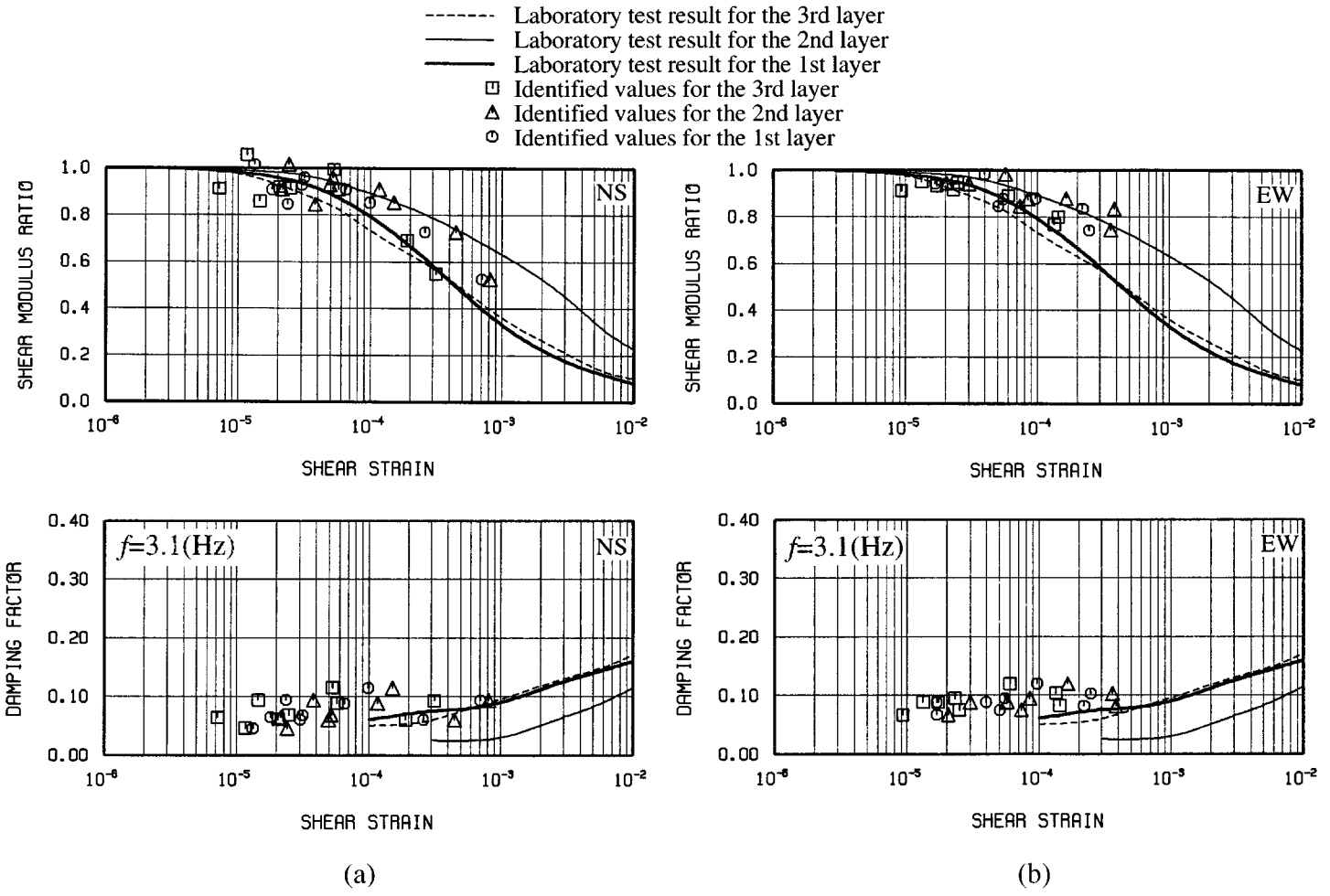

Figure 9. Relation between the effective shear strain and the shear modulus reduction ratio or the damping factor for (a) the NS component and (b) the EW component

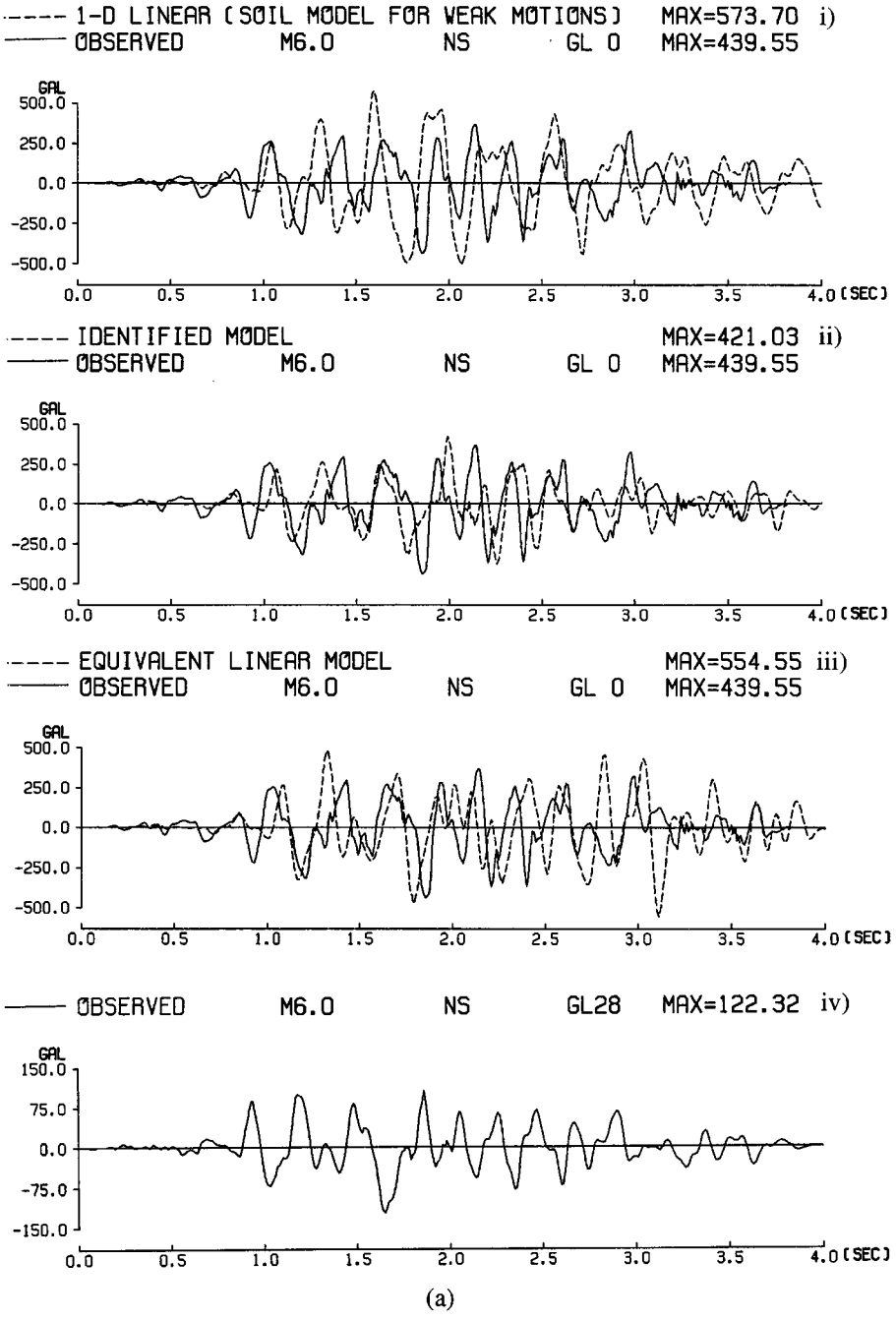

Figure 10. Comparison between observed (solid lines) and simulated (dashed lines) waveforms of (a) the NS component of No. 9, and (b) the NS component of No. 37

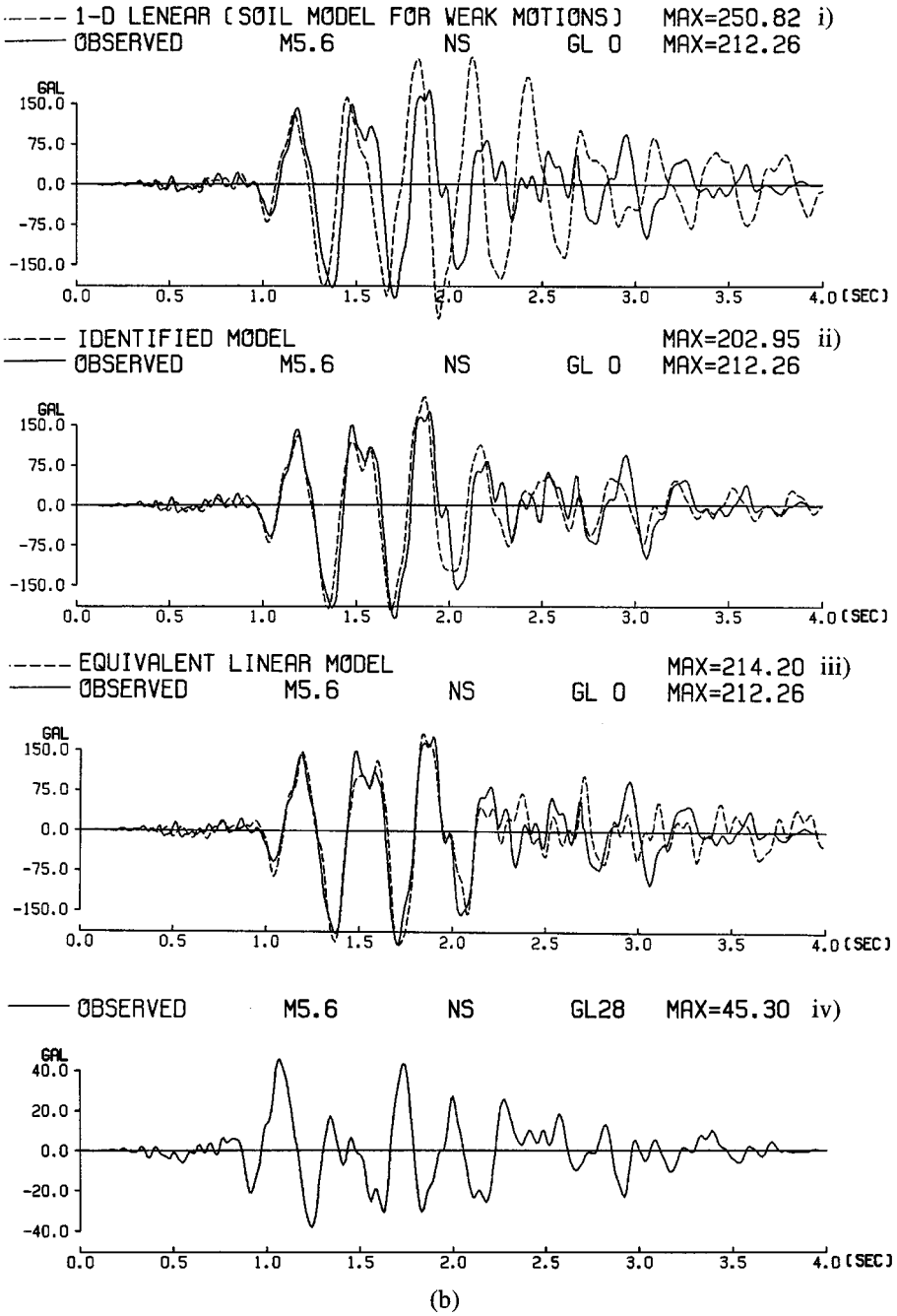

(b)

Figure 10. (Continued)

4.3. Simulation of strong motions

In order to examine if the equivalent linear 1-D model using the dynamic deformation characteristics obtained from laboratory tests is useful for strong motion prediction, we simulated strong motions at GL0, using records at GL28 as input motions, based on the following three methods. These are (i) a linear 1-D model using the average of soil constants identified from weak motions, (ii) a linear 1-D model using soil constants identified from the strong motion of interest, and (iii) an equivalent linear 1-D model using the average of soil constants identified from weak motions and dynamic deformation characteristics obtained from laboratory tests. We use frequency-dependent damping factors for the equivalent linear 1-D model as well as the linear 1-D model by modifying the program by Schnabel *et al.*[25] In the modified program,[27] we assume that h_0 depends on the effective shear strain based on laboratory test results and that α is a constant value, the average of the estimates from weak motions as shown in Table III.

The observed waveforms and simulated ones at GL0 are shown in Figure 10. It is confirmed that (i) overestimates the observed waveforms, while (ii) can explain the observed waveforms best among the three. It is found that (iii) can explain the NS component of No. 37 with an effective shear strain of 4×10^{-4} very well. For the NS component of No. 9 with an effective shear strain of 8×10^{-4}, (iii) can explain the strong motion better than (i), but still overestimates the observed waveform. Examining waves for NS component of No. 9 closely, it is found that the phase at a time of 1·0 s is explained better by (i) than by (ii), but the phase after the time of 1·5 s is explained better by (ii) than by (i). This result means that non-linearity becomes clear after the time of 1·5 s for the NS component of No. 9. The result shown in Figure 4 that the peak of cross-correlation for the NS component of No. 9 is not as clear as the peaks for the others at a time lag of $-0{\cdot}12$ s might be explained, namely, by the time-varying non-linearity of soil. Summarizing these results, we can say that the equivalent linear 1-D model is valid enough to simulate strong motions, at least at an effective shear strain of less than 4×10^{-4} if we use S-wave velocities and frequency-dependent damping factors identified from weak motions and dynamic deformation characteristics obtained from laboratory tests.

5. CONCLUSIONS

We evaluate the non-linear behaviour of soil sediments by analysing weak and strong motions observed at depths of 1 m (GL0) and 28 m (GL28), in eastern Shizuoka prefecture, Japan. We analyse horizontal components for nine earthquakes, four strong motions, whose larger PGA of NS and EW components is greater than 100 cm/s^2 and five weak motions, whose PGAs are between 10 and 40 cm/s^2.

(1) We calculate spectral ratios of S-wave segments with a duration of 3 s between GL0 and GL28. As a result, the spectral ratios of strong motions whose PGAs are 440, 210, 176 and 140 cm/s^2 show clear shifts of their peaks to a longer-period compared with the peaks of weak motions.
(2) We identify S-wave velocities and frequency-dependent damping factors $h = h_0 f^{-\alpha}$ to minimize the residual between observed and theoretical spectral ratios based on a linear 1-D model. We show that S-wave velocities identified from strong motions whose PGAs are 440, 210, 176, and 140 cm/s^2 are significantly smaller than those identified from weak motions.
(3) We estimate the effective shear strain, which is 65 per cent of the maximum shear strain, based on a linear 1-D model using identified soil constants. It is found that the shear modulus reduction ratios estimated from identified S-wave velocities become clear above an effective shear strain of 10^{-4} and agree with laboratory test results below an effective shear strain of 8×10^{-4}.
(4) For identified frequency-dependent damping factors, we cannot see clear differences between weak and strong motions below an effective shear strain of 8×10^{-4} as the laboratory test suggested.
(5) We simulate strong motions at GL0 using records at GL28 as input motions based on the equivalent linear 1-D model. It is found that the equivalent linear 1-D model is valid enough to simulate strong

motions, at least an effective shear strain of less than 4×10^{-4} if we use S-wave velocities and frequency-dependent damping factors identified from weak motions and dynamic deformation characteristics obtained from laboratory tests.

REFERENCES

1. H. B. Seed and I. M. Idriss, 'The influence of soil conditions on ground motions during earthquake', *J. soil mech. foundations div. ASCE* **94**, 93–137 (1969).
2. H. B. Seed and I. M. Idriss, 'Soil moduli and damping factors for dynamic response analysis', Report EERC 70-10, Earthquake Engineering Research Center, University of California, Berkely, 1970.
3. B. O. Hardin and V. P. Drnevich, 'Shear modulus and damping in soil: measurement and parameter effects', *J. soil mech. foundations div. ASCE* **98**, 603–624 (1972).
4. B. O. Hardin and V. P. Drnevich, 'Shear modulus and damping in soil: design equations and curves', *J. soil mech. foundations div. ASCE* **98**, 667–692 (1972).
5. W. B. Joyner, R. E. Warrick and T. E. Fumal, 'The effects of Quaternary alluvium on strong ground motion in the Coyote Lake, California earthquake of 1979', *Bull. seism. soc. Am.* **71**, 1333–1349 (1981).
6. B. E., Tucker and J. L. King, 'Dependence of sediment-filled valley response on input amplitude and valley properties', *Bull. seism. soc. Am.* **74**, 153–165 (1984).
7. B. H. Chin and K. Aki, 'Simultaneous study of the source, path and site effects on strong ground motion during the 1989 Loma Prieta earthquake: a preliminary result on pervasive nonlinear site effects', *Bull. seism. soc. Am.* **81**, 1859–1884 (1991).
8. M. Kamiyama, 'Non-linear soil amplification identification empirically from strong earthquake ground motions', *J. phys. earth* **40**, 151–173 (1992).
9. M. Yamamoto, T. Iwata and K. Irikura, 'Estimation of site effects for strong and weak ground motions at Kushiro local meteorological observatory', *Zishin* **48**, 341–351 (1995) (in Japanese with English abstract).
10. S. K. Singh, J. Lermo, T. Dominguez, M. Ordaz, J. M. Espinosa, E. Mena and R. Quaas, 'The Maxico earthquake of September 19, 1985 — a study of amplification of seismic waves in the Valley of Mexico with respect to a hill zone site', *Earthquake spectra* **4**, 653–673 (1988).
11. A. Figueras, A. Roca and X. Goula, 'Larger soil amplification for stronger ground motion from SMART-1 records', in *Proc. 10th world conf. earthquake eng*., Rotterdam, (1992), pp. 1043–1047.
12. I. A. Beresnev, K.-L. Wen and Y. T. Yeh, 'Nonlinear soil amplification: Its corroboration in Taiwan', *Bull. seism. soc. Am.* **85**, 496–515 (1995).
13. C. Y. Chang, C. M. Mok, M. S. Power, Y. K. Tang, H. T. Tang and J. C. Stepp, 'Development of shear modulus reduction curves based on Lotung downhole ground motion data', in *Proc. 2nd intel. conf. on recent advances in geotechnical earthquake engineering and soil dynamics*, St. Louis, Missouri, 1991, pp. 111–118.
14. K. L. Wen, 'Non-linear soil response in ground motions', *Earthquake Engng. Struct. Dyn.* **23**, 599–608 (1994).
15. T. Satoh, T. Sato and H. Kawase, 'Nonlinear behavior of soil sediments identified by using borehole records observed at the Ashigara Valley, Japan', *Bull. seism. soc. Am.* **85**, 1821–1834 (1995).
16. R. B. Darragh and A. F. Shakal, 'The site response of two rock and soil station pairs to strong and weak ground motion', *Bull. seism. soc. Am.* **81**, 1885–1899 (1991).
17. K. L. Wen, I. A. Beresnev and Y. T. Yeh, 'Investigation of non-linear site amplification at two downhole strong ground motion arrays in Taiwan', *Earthquake Engng. Struct. Dyn.* **24**, 313–324 (1995).
18. S. Midorikawa, 'Nonlinearity of site amplification during strong ground shaking', *Zishin* **46**, 207–216 (1993) (in Japanese with English abstract).
19. K. Egawa, S. Kondo, I. Katayama, K. Ozeki and I. Yoshida, 'Study on surface and borehole strong motion records during the Eastern Yamanashi prefecture earthquake of 1983', *Program and Abstracts*, The Seismological Society of Japan, **2** (1985) p. 139 (in Japanese).
20. F. Yamazaki, L. Lin and T. Katayama, 'Orientation error estimation of buried seismographs in array observation', *Earthquake Engng. Struct. Dyn.* **21**, 679–694 (1992).
21. H. Kawase and T. Sato, 'Simulation analysis of strong motions in the Ashigara Valley considering one- and two-dimensional geological structures', *J. phys. earth* **40**, 27–56 (1992).
22. G. A. Bekey, 'System identification — an introduction and a survey', *Simulation* **15**, 151–166 (1970).
23. Y. Ohta, 'Application of optimization technique for earthquake engineering', *Trans. architect. inst. Japan* **299**, 35–41 (1975) (in Japanese)
24. T. Satoh, H. Kawase and T. Sato, 'Evaluation of local site effects and their removal from borehole records observed in the Sendai region, Japan', *Bull. seism. soc. Am.* **85**, 1770–1789 (1995).
25. P. B. Schnabel, J. Lysmer and H. B. Seed, 'SHAKE — a computer program for earthquake response analysis of horizontally layered sites', *Report EERC 72-12*, Earthquake Engineering Research Center, University of California, Berkely, 1972.
26. R. Fletcher, 'FORTRAN subroutines for minimization by quasi-Newton methods', *Report R7125 AERE*, Harwell, England, 1972.
27. T. Satoh, H. Kawase and T. Sato, 'Strong motion prediction considering both non-linear behavior of soil and the statistical characteristics of ground motion extracted from observed data', *J. struct. constr. eng.* **463**, 27–37 (1994) (in Japanese with English abstract).

